Environmental Technology

ISSN: 0959-3330 (Print) 1479-487X (Online) Journal homepage: www.tandfonline.com/journals/tent20

Enhanced struvite production via membrane capacitive deionization and electrolysis: interference of humic acid and calcium

Aditya Kurnia Aji Pangestu, Arseto Yekti Bagastyo, Ervin Nurhayati, Jr-Lin Lin & Fahrudin Sidik

To cite this article: Aditya Kurnia Aji Pangestu, Arseto Yekti Bagastyo, Ervin Nurhayati, Jr-Lin Lin & Fahrudin Sidik (28 Aug 2025): Enhanced struvite production via membrane capacitive deionization and electrolysis: interference of humic acid and calcium, Environmental Technology, DOI: 10.1080/09593330.2025.2549531

To link to this article: https://doi.org/10.1080/09593330.2025.2549531

View supplementary material

Published online: 28 Aug 2025.

Submit your article to this journal

Article views: 3

View related articles

View Crossmark data

Full Terms & Conditions of access and use can be found at
https://www.tandfonline.com/action/journalInformation?journalCode=tent20

ENVIRONMENTAL TECHNOLOGY
https://doi.org/10.1080/09593330.2025.2549531

Taylor & Francis
Taylor & Francis Group

Check for updates

Enhanced struvite production via membrane capacitive deionization and electrolysis: interference of humic acid and calcium

Aditya Kurnia Aji Pangestu[a], Arseto Yekti Bagastyo [a], Ervin Nurhayati [a], Jr-Lin Lin[b] and Fahrudin Sidik [b,c]

[a]Department of Environmental Engineering, Faculty of Civil, Planning, and Geo-Engineering, Institut Teknologi Sepuluh Nopember, 60111, Surabaya, Indonesia; [b]Department of Environmental Engineering, Chung Yuan Christian University, Chung-Li, Taiwan; [c]Department of Civil Engineering, Chung Yuan Christian University, Chung-Li, Taiwan

ABSTRACT

This study examined struvite crystal formation for nutrient recovery in the presence of coexisting cations and organic substances. Coupled membrane capacitive deionization (MCDI) with sacrificial magnesium anode electrolysis was performed to produce struvite crystals from synthetic wastewater containing ammonium, phosphate, sodium, calcium, and humic acid (HA). In this way, MCDI was employed to adsorb coexisting cations onto the activated carbon (AC) electrode and retain NH_4^+ and PO_4^{3-} ions in the effluent. The MCDI effluent was the input for Mg-based electrolysis, which used an AZ31B Mg alloy as the anode to release Mg^{2+} ions. Various initial Nitrogen/Phosphate (N/P) molar ratios were prepared (i.e. 1:1, 5:1, and 10:1) in the absence and presence of 10 mM competitor ions and 100 mg·L^{-1} of HA. The results showed that MCDI can retain NH_4^+ and PO_4^{3-} approximately 84.19 and 78.07%, respectively, which is equivalent to the ion electrosorption capacity of the AC electrode, approximately 15.53 mg·g^{-1} for NH_4^+ and 21.45 mg·g^{-1} for PO_4^{3-}. Interestingly, the addition of co-ions, such as Na^+ and Ca^{2+}, can remain 2–5 times NH_4^+ and PO_4^{3-} in the effluent. After Mg-based electrolysis, NH_4^+ and PO_4^{3-} ions increased by approximately 87.32% and 63.65%, respectively. In the presence of Na^+, coupling MCDI with the electrolysis process produced up to 0.6195 g of high-purity struvite. Conversely, HA and Ca^{2+} significantly reduced crystal purity and altered morphology. Under an N/P ratio of 10:1, without co-ions or humic acid, the energy consumption for struvite recovery was 15.88 Wh g^{-1}.

ARTICLE HISTORY
Received 26 May 2025
Accepted 13 August 2025

KEYWORDS
Ammonium; electrolysis-magnesium anode; MCDI; phosphate; struvite

1. Introduction

Conventional methods for removing ammonium (NH_4^+) and phosphate (PO_4^{3-}) from wastewater rely on biological and chemical processes. NH_4^+ is typically removed through nitrification and denitrification, which convert it into gaseous nitrogen (N_2), whereas PO_4^{3-} ions is commonly eliminated via chemical precipitation or biological treatment [1,2]. Biological treatment can achieve NH_4^+ and PO_4^{3-} ions removal efficiencies of up to 85.5% and 60%, respectively [3]. However, these processes often require substantial infrastructure investment, high operational and maintenance costs, and a large land area, limiting their scalability and sustainability [1,4]. Electrochemical separation has emerged as a promising alternative for water purification and resource recovery, including NH_4^+

CONTACT Arseto Yekti Bagastyo bagastyo@enviro.its.ac.id Department of Environmental Engineering, Faculty of Civil, Planning, and Geo-Engineering, Institut Teknologi Sepuluh Nopember, 60111, Surabaya, Indonesia; Jr-Lin Lin jrlin@cycu.edu.tw Department of Environmental Engineering, Chung Yuan Christian University, Chung-Li, Taiwan

Supplemental data for this article can be accessed online at https://doi.org/10.1080/09593330.2025.2549531.

© 2025 Informa UK Limited, trading as Taylor & Francis Group

and PO_4^{3-}, due to its simplicity, energy efficiency, and environmental friendliness. Various electrochemical methods have been explored, including membrane-based systems, electrocoagulation, and internal micro-electrolysis. Among these, membrane-based electrochemical techniques demonstrate superior performance and energy efficiency, making them particularly promising for NH_4^+ and PO_4^{3-} recovery [5].

Membrane capacitive deionization (MCDI) has recently emerged as an effective electrochemical technique for removing a wide range of pollutants, such as inorganic salts and nutrient ions, from water. MCDI is a membrane-based system incorporating a pair of ion exchange membranes and a porous electrode. These membranes regulate ion transport, enhancing the selectivity and efficiency of target-ion separation and recovery from feed solutions [6]. Several studies have demonstrated that MCDI can achieve removal efficiencies of up to 89% for NH_4^+ and 57.5% for PO_4^{3-} using an activated carbon (AC) electrodes operated at applied voltage between 1–2 V, in combination with various ion exchange membranes, such as IONSEP MC and Membrain [7–9]. Although MCDI exhibits promising removal performance, energy consumption remains a critical factor influencing its operational feasibility and cost-effectiveness. The voltage and current efficiency were the key parameters affecting the energy usage. Excessive voltage can trigger water electrolysis, significantly reducing energy efficiency and increasing overall operational costs. Therefore, optimizing operational parameters is essential for maximizing nutrient recovery and energy efficiency [5].

NH_4^+ and PO_4^{3-} are essential nutrients becoming scarce in natural environments due to rising global demand from agricultural and ecological systems. One promising approach to reclaiming these valuable resources is through the formation of struvite ($MgNH_4PO_4{\cdot}6H_2O$, MAP), a slow-release fertilizer composed of magnesium (Mg), NH_4^+, and PO_4^{3-}. Struvite has gained significant attention as a sustainable fertilizer that addresses both agricultural productivity and global phosphorus management challenges. Unlike conventional PO_4^{3-} fertilizer, struvite is recovered from wastewater streams, offering a valuable route for phosphorus recycling and reducing reliance on finite PO_4^{3-} rock reserves, which are under increasing pressure due to global food demand [10]. Because of its slow-release characteristics, crops are ensured a consistent supply of phosphorus and nitrogen, reducing nutrient losses from leaching and runoff, which further improves the efficiency of fertilizer utilization [10–12].

Studies have demonstrated that struvite can provide yields and nutrient uptake comparable to traditional fertilisers while reducing the risk of root burn and heavy metal contamination, making it suitable for a wide range of crops and soil types [12,13]. The adoption of struvite not only supports circular economy principles but also contributes to food security and environmental protection by closing the nutrient loop and mitigating eutrophication risks. Given the global urgency for sustainable phosphorus recovery and the increasing cost of conventional fertilisers, struvite represents a promising solution for future agricultural systems [10].

Several factors, including pH, supersaturation levels, and the molar ratios of the involved ions, influence struvite precipitation [14]. Numerous studies have demonstrated that struvite crystallization using a stirred tank reactor (STR) can achieve removal efficiencies of over 80% for both NH_4^+ and PO_4^{3-} [15]. A key factor in struvite production is the selection of a suitable Mg source, which significantly affects both the product quality and overall production cost.

The familiar sources of Mg for chemical-based struvite precipitation, including $MgCl_2$, $MgSO_4$, $Mg(OH)_2$, MgO, seawater, magnesite, and Mg alloys, have distinct advantages and limitations. Generally, chemically derived Mg sources are costly and often lead to unwanted by-products. Mg alloys are metallic materials composed primarily composed of Mg alloyed with elements such as aluminum (Al) and zinc (Zn) to enhance their mechanical and electrochemical properties. Because its low standard reduction potential among common engineering metals (e.g. Al, Zn, Fe, Cu, and Ni), Mg is highly reactive and suitable for use as a sacrificial anode in electrochemical system. At such a conditions, Mg alloys undergo anodic dissolution, realizing Mg^{2+} ions into the solution while simultaneously generating hydrogen (H_2) gas. Utilizing Mg alloys as material electrode as alternative can minimize the dependencies on conventional chemical reagents such as $MgCl_2$, $MgSO_4$, and $Mg(OH)_2$, which are often costly and generate undesirable by-products [16]. Several studies have demonstrated the feasibility of this approach. For example, Hug & Udert [35] pioneered electrolysis with a Mg sacrificial anode, achieving PO_4^{3-}removal efficiencies of 59-84% at an initial pH of 8.9. Recently, Luo et al. [17] reported PO_4^{3-} recovery rates of 5.24 mg-P·h^{-1}·cm^{-2} in artificial digestion fluid and 4.60 mg-P·h^{-1}·cm^{-2} in anaerobically digested chicken manure slurry over a 90-min. These results confirm the feasibility of utilizing Mg alloys as sacrificial anodes in electrochemical systems for nutrient recovery via struvite precipitation.

Traditionally, MCDI and Mg-based anode electrolysis have been performed independently, achieving distinct nutrient removal and recovery performance. However, combining these two technologies offers the potential

for synergistic enhancement, enabling improved recovery of NH_4^+ and PO_4^{3-} while optimizing energy efficiency. Using Mg alloy as a sacrificial anode is particularly advantageous due to its cost-effectiveness and low formation of by-products. Given the demonstrated performance of standalone MCDI and electrolysis systems for nutrient removal from various wastewater sources, this study investigates the integration of these two processes for recovering NH_4^+ and PO_4^{3-} in the form of struvite precipitate from synthetic wastewater. In the MCDI experiments, parameters such as NH_4^+ and PO_4^{3-} removal rates, electrosorption capacity, and energy consumption were evaluated. In the electrolysis experiments, the nutrient removal efficiency, energy consumption, struvite purity, and crystal morphology were assessed.

2. Materials and methods

2.1. Artificial wastewater preparation

A synthetic wastewater solution (600 mL) was prepared by dissolving NH_4Cl (Honeywell) and K_2HPO_4 (Sigma-Aldrich) as the primary sources of NH_4^+ and PO_4^{3-}, respectively, in distilled water. To simulate competitive conditions, sodium chloride (NaCl; Sigma-Aldrich) and $CaCl_2$ (J.T. Baker) were added as sources of competing cations, while humic acid (HA) (Local brand, experimental grade with 99% purity) was added as a representative organic substance. The concentrations of these components were varied according to the experimental design.

2.2. Experimental setup

2.2.1. MCDI setup

The MCDI reactor consisted of a single compartment containing three-unit cells connected in series. Each unit cell included titanium current collectors ($90 \times 70 \times 1$ mm) coated with AC electrodes (surface area: 24 cm^2) and paired with ion-exchange membranes. The electrode spacing was maintained at 2 mm. Anion (Ionsep-AEM) and cation (Ionsep-CEM) exchange membranes, each measuring $90 \times 70 \times 4$ mm, were supplied by Hangzhou Iontech Environmental Technology Co., Ltd. A polymer spacer was placed between the membranes to prevent adhesion. Acrylic end plates ($140 \times 120 \times 20$ mm) enclosed the reactor, and rubber seals were used throughout to prevent leakage. The AC coating was prepared by mixing N, N-dimethylacetamide (DMAc) (Thermo Scientific), polyvinylidene fluoride (PVDF) (Thermo Scientific), and AC (Sigma-Aldrich, particle size of 150 μm) in a 9:1:3 weight ratio. The dry masses of AC on the anode and cathode were 0.97 and 0.98 g, respectively. A direct current (DC) power supply (Sugon 3005D, China) was used to power the electrodes. A 600 mL of feed solution was circulated in a batch test mode using a peristaltic pump (DGS DG600LV3, China) at a flowrate of 5 $mL \cdot min^{-1}$. The initial pH was adjusted to 7 to simulate neutral conditions, and a constant voltage of 1.2 V was applied for 90 min (Figures 1 and 2). Pre-experiments were conducted to obtain the optimum condition for constant voltage and operational time.

2.2.2. Electrolysis setup

The electrolysis reactor comprised a 600 mL glass beaker serving as the main compartment, along with an electrode hanger to support the electrodes. An AZ31B Mg alloy plate (dimensions: $100 \times 49 \times 1.2$ mm, locally sourced) was used as the sacrificial anode, while a 316 stainless steel (316SS) plate of the exact dimensions served as the cathode. Those electrodes were assembled 2 cm apart and connected to a DC power supply. A 600 mL feed solution was circulated using a peristaltic pump (DGS DG600LV3, China) at a constant 10 $mL \cdot min^{-1}$ flow rate. The pH of the solution was adjusted and maintained within the range of 6.0 to 8.0 ± 0.5 (Figure 3). The experiment was conducted for 30 min at a constant current of 0.7 A. The constant current and operational time were determined based on the optimal conditions from the preliminary test.

2.3. Analytical methods

2 mL samples were collected at the initial and end of experiment to further quantify NH_4^+ and PO_4^{3-} concentrations. NH_4^+ concentration was determined by Nessler method, and PO_4^{3-} concentrations by standard L-ascorbic acid methods. Samples were then analyzed using a UV-Vis spectrophotometer (Thermo Fisher Scientific Genesys 20, USA) to the appropriate wavelengths for each measurement. The morphology and purity of the struvite precipitate were examined using field emission scanning electron microscopy coupled with energy-dispersive X-ray spectroscopy (SEM-EDX, FEI Inspect S50, USA) and X-ray diffraction (XRD, X'Pert PRO, PANalytical, Netherlands), respectively.

The removal efficiency (η, %) of NH_4^+ and PO_4^{3-} was calculated using Equations (1) and (2), while the electrosorption capacities of N_2 and PO_4^{3-} (q_e, $mg \cdot g^{-1}$) were determined using Equations (3) and (4).

$$\eta = \frac{C_{0N} - C_{tN}}{C_{0N}} \times 100\% \quad (1)$$

$$\eta = \frac{C_{0P} - C_{tP}}{C_{0P}} \times 100\% \quad (2)$$

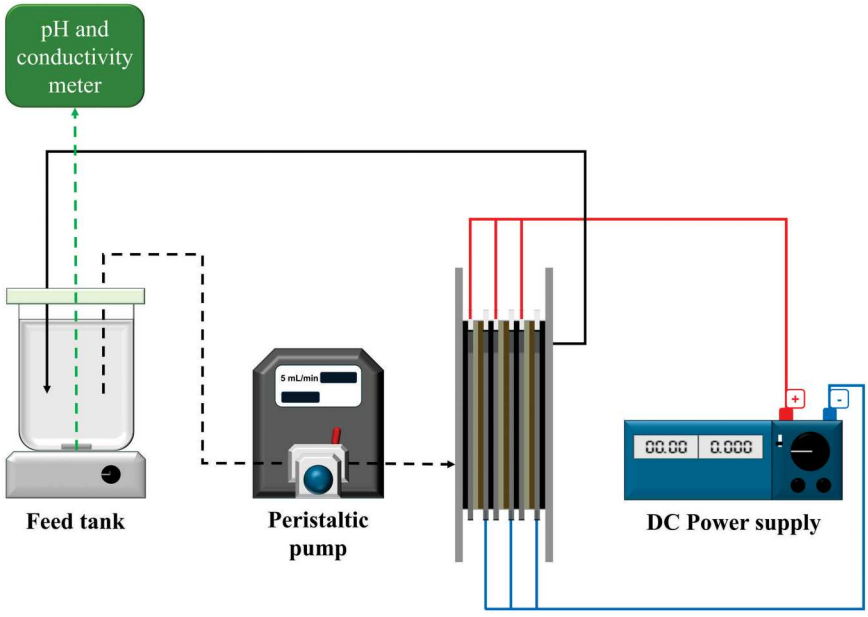

Figure 1. Schematic of the MCDI experiment.

where C_{0N} and C_{tN} (mg·L^{-1}) are the initial and final NH_4^+ concentrations, respectively while C_{0P} and C_{tP} (mg·L^{-1}) are the initial and final PO_4^{3-} concentrations, respectively.

$$q_e = \frac{C_{0N} - C_{tN}}{M} \times V \quad (3)$$

$$q_e = \frac{C_{0P} - C_{tP}}{M} \times V \quad (4)$$

where C_{0N} and C_{tN} (mg·L^{-1}) are the initial and final NH_4^+ concentrations, V (L) is the volume of solutions; and M (g) is the mass of active material in the cathode while C_{0P} and C_{tP}(mg·L^{-1}) are the initial and final PO_4^{3-} concentrations, V (L) is the volume of solutions; and M (g) is the mass of active material in the anode.

The energy input (E_c, Wh) was calculated using Equations (5) and (6). Equation (5) was applied for the constant voltage system, whereas Equation (6) was

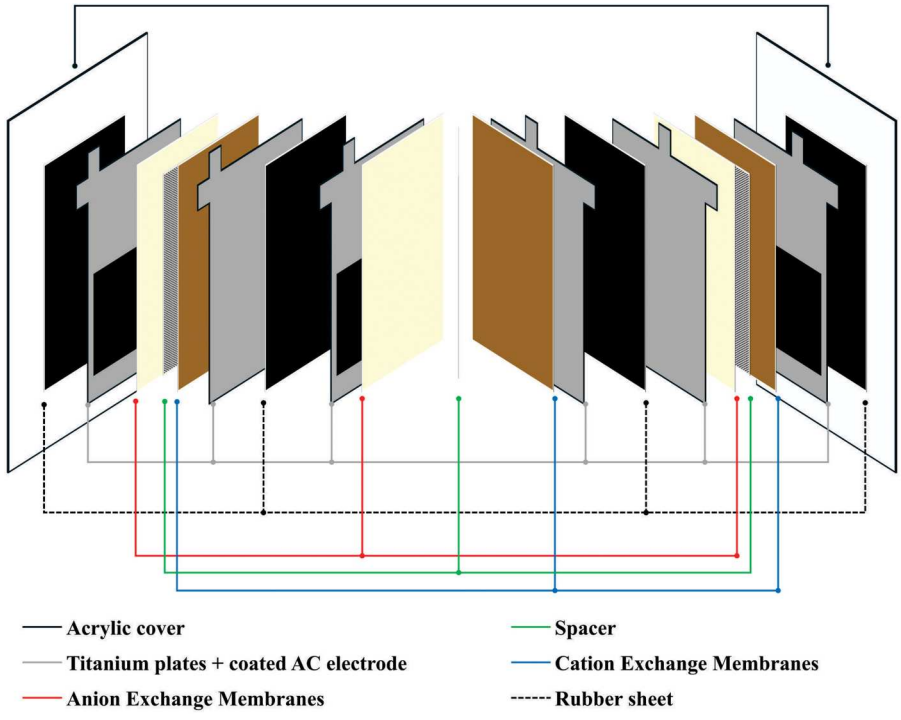

Figure 2. MCDI configuration details.

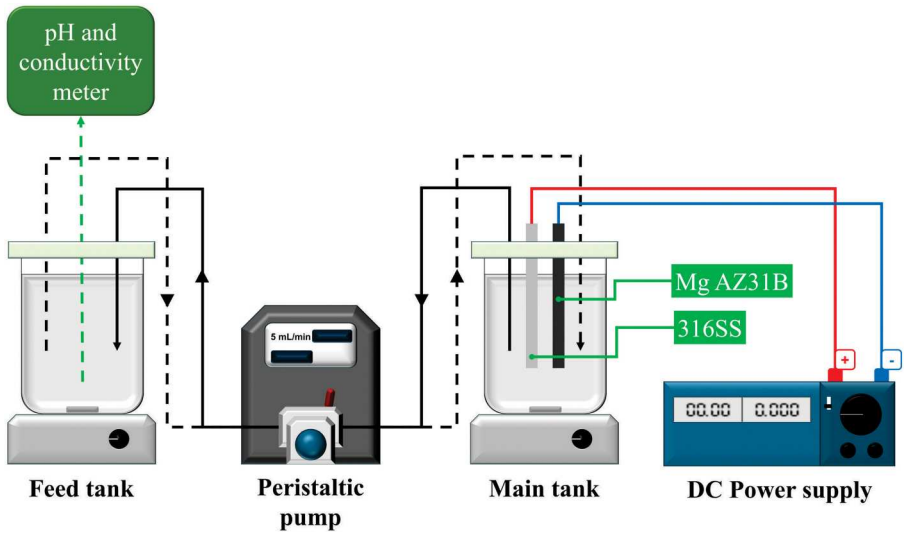

Figure 3. Schematic of the electrolysis experiment.

used for the constant current system [18].

$$E_c = V \times \int_0^t Idt \tag{5}$$

$$E_c = I \times \int_0^t Vdt \tag{6}$$

where V (V) is the applied voltage and I (A) is the current.

3. Results and discussion

3.1. Ammonium and phosphate removal by MCDI and electrolysis

To evaluate the adsorption behaviour and selectivity of NH_4^+ and PO_4^{3-} in the presence of competing ions (Na^+ and Ca^{2+}) and HA, MCDI was conducted at varying N/P molar ratios at different concentrations of co-ions, with and without HA addition, as shown in Figure 4. This result showed that the presence of stand-alone Na^+ and Ca^{2+} or their mixtures significantly influenced the electrosorption of NH_4^+ onto the AC electrode. This was evidenced by the high remaining NH_4^+ concentration in the effluent in the range of 91.76–96.61% compared to that of the original (84.19%) after the MCDI test with an initial N/P molar ratio of 1:1 (Figure 4(a)).

The performance of MCDI was assessed by measuring the residual concentrations of NH_4^+ and PO_4^{3-} in the effluent, particularly in the presence of competing ions such as Na^+ and Ca^{2+}, as well as organic matter in the form of HA. The MCDI-treated effluent was then subjected to electrochemical treatment using a Mg anode to facilitate the synthesis of struvite as the final product. This phenomenon was associated with a 2–5-fold reduction in electrosorption capacity compared to the original conditions (15.53 mg g^{-1}). The reduced NH_4^+ adsorption can be attributed to the preferential electrosorption of Na^+ over NH_4^+ because the hydrated radii of Na^+ (3.58 Å) are larger than those of NH_4^+ (3.31 Å). Under such conditions, Na^+ formed a stronger electric double layer (EDL), enhancing the overlapping effects [19,20]. Similarly, the preferential adsorption of Ca^{2+} ions over NH_4^+ was also observed due to the divalent nature of Ca^{2+}, which enables stronger electrostatic interactions with the negatively charged electrode surface compared to the monovalent NH_4^+, allowing more effective surface charge neutralization [8]. These findings were consistent with those of another study [21], which showed that the EDL overlapping effect became more pronounced with increasing hydrated ion radii, making it more challenging for ions with larger hydrated radii to reach the electrode surface. In addition, it has been widely reported that divalent ions tend to exhibit more dominant adsorption behaviour than monovalent ions.

In the case of PO_4^{3-}, electrosorption trends varied depending on the N/P molar ratio and the presence of HA. In the absence of HA, PO_4^{3-} adsorption remained relatively stable in the presence of competing cations (Na^+ and Ca^{2+}) at an N/P molar ratio of 1:1, indicating minimal interference from thus co-ions. However, as the N/P ratio increased to 5:1 (Figure 4(c,d)) and 10:1 (Figure 4(e–f)), the electrosorption capacity for PO_4^{3-} consistently declined. This decline was likely due to the reduced initial availability of PO_4^{3-} at higher N/P ratios, which constrained its uptake despite stable adsorption conditions. In contrast, the presence of 100 mg·L^{-1} of HA slightly altered the PO_4^{3-} electrosorption across all N/P ratios. At such conditions, the strongly negative charged functional groups on HA could

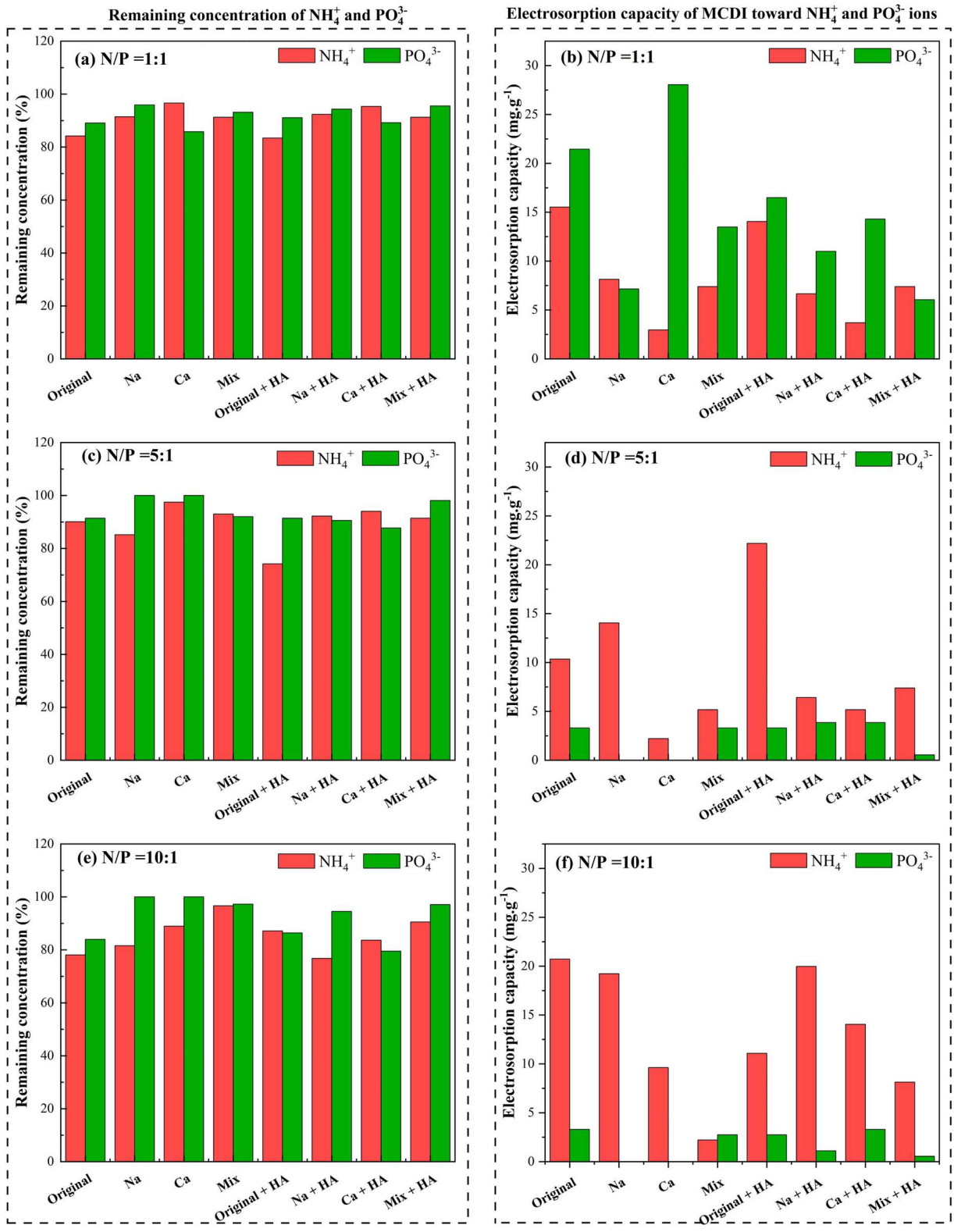

Figure 4. Remaining concentration (left panels) and electrosorption capacities (right panels) of NH_4^+ and PO_4^{3-} after MCDI at different molar ratios of N/P: (a-b) 1:1, (c-d) 5:1, (e-f) 10:1. Experiments were conducted at 1.2 V and 7 pH conditions for 90 min with an initial NH_4^+ concentration of 10 mM.

interact with multivalent cations, such as Ca^{2+}, thereby facilitating the transport of NH_4^+ and PO_4^{3-} passing through membranes and slightly increasing their adsorption onto the electrode surface. A previous study revealed that HA compounds can partially adsorb onto the membrane surface or infiltrate

membrane pores, potentially modulating the transport of larger ions [22,23]. Although the initial N/P molar ratios were fixed at 5:1 and 10:1, the electrosorption capacity for PO_4^{3-} decreased with increasing ratios, likely due to reduced PO_4^{3-} availability. Regardless, the presence of HA and co-ions ultimately resulted in limited electrosorption of both NH_4^+ and PO_4^{3-}, leaving higher concentrations of these ions in the solution after MCDI treatment. This remaining ion content in the effluent is beneficial for subsequent Mg-based electrolysis, as it provides an adequate supply of NH_4^+ and PO_4^{3-}, necessary for efficient struvite crystallization.

The removal of NH_4^+ and PO_4^{3-} was further evaluated during electrolysis to understand their reactivity with the released Mg^{2+} toward struvite crystal formation. A previous study [24] investigated the crystallization of struvite, revealing that a molar ratio of NH_4^+:PO_4^{3-}: Mg^{2+} of roughly 1:1:1 facilitates the removal of NH_4^+ and PO_4^{3-} by approximately 83.60% and 99.91%, respectively. Figure 5(a) showed that NH_4^+ and PO_4^{3-} removal at Original variation with an initial N/P molar ratio of 1:1 was 87.32% and 63.65%, respectively. However, additional coexisting ions such as Na^+ or Ca^{2+} decreased NH_4^+ and PO_4^{3-} removal in the ranges of 9.37–45.42% and 43.38–61.99%, respectively. Similarly, the Mix variation exhibits a lower NH_4^+ removal efficiency, approximately 28.74%, compared to the Original at 83.09%. In such a condition, the slight decrease in NH_4^+ and PO_4^{3-} removal was likely due to the presence of Na^+, Ca^{2+}, and HA in the MCDI effluent following the treatment process. Although the overall concentrations of NH_4^+ and PO_4^{3-} remained 4–5 times higher than those of the coexisting ions and HA, the presence of these substances can still act as impurities, interfering with the reaction among Mg, NH_4, and PO_4 during struvite crystallization. Moreover, this inhibitory effect was consistently observed across all variations in the N/P molar ratio during the electrolysis process (Figure 5(b,c)).

3.2. Effect of ammonium/phosphate molar ratio on the precipitate

Following the electrolysis process, the dry mass of the precipitates was quantified to assess the influence of the N/P molar ratio on precipitate formation (Figure 6). The results showed that the Original variation, with an initial N/P molar ratio of 1:1, produced 1.40 g of precipitate. The introduction of co-existing ions and HA led to an increase in the dry mass precipitates, ranging from 1.48 to 1.82 g. The highest yield, 1.83 g, was achieved in the presence of both Na^+ ions and HA. Interestingly, in the absence of HA, the precipitate mass was approximately 10–20% higher compared to the Original samples, suggesting that HA plays a significant role in facilitating the incorporation of co-existing ions during precipitation [25]. However, increasing the initial N/P molar ratio to 5:1 and 10:1 led to a decline in precipitate formation efficiency. This indicates that maintaining a stoichiometric balance between nitrogen and phosphorus is essential for optimal precipitation. Overall, these findings highlight the significant impact of the N/P ratio on precipitate yield while also demonstrating that co-existing ions and HA contribute to enhanced ion incorporation and precipitation efficiency.

3.3. Characterization of crystals formed after MCDI and electrolysis processes

Two possible mechanisms may explain the observed precipitation behaviour in this study. First, the competing ions introduced into the system may have been efficiently removed during the MCDI process, resulting in an NH_4^+ and PO_4^{3-} enriched effluent. This relatively 'purified' ionic ecosystem would increase the likelihood of struvite formation during subsequent electrolysis. Alternatively, some competing ions may have bypassed the MCDI separation and remained in the effluent, potentially leading to the formation of mixed-phase or non-struvite precipitates. To clarify the nature of the resulting solids, the morphology and elemental composition of the precipitates were analyzed using SEM-EDX, whereas their crystalline phases were identified through XRD analysis.

3.3.1. Scanning Electron Microscopy (SEM) imaging of the formed crystals

The identification of struvite crystals (highlighted in red marks) in the SEM images observation (Figures 7 and 8) was based on morphological comparison with previously reported crystal structures [25]. In this a previous study, struvite typically forms well-defined, prismatic or rod-like crystals with a needle-like appearance, consistent with the morphology observed in Figure 7(a). This characteristic morphology was also observed in the presence of Na^+, Ca^{2+}, or their combination (Figure 7(b–d)). However, the introduction of HA significantly altered crystal formation. In all HA-containing variations (Original + HA, Na + HA, Ca + HA, and Mix + HA), struvite crystals exhibited less regular shapes, including trapezoidal prisms and pyramid-like forms (Figure 8(a–d)). This morphological transformation is attributed to HA adsorption onto active growth sites on the crystal surface, which inhibited the development of specific crystals faces and led to reduced particle sizes. These effects indicate that HA interference with both the nucleation and growth kinetics of struvite crystals [25–28].

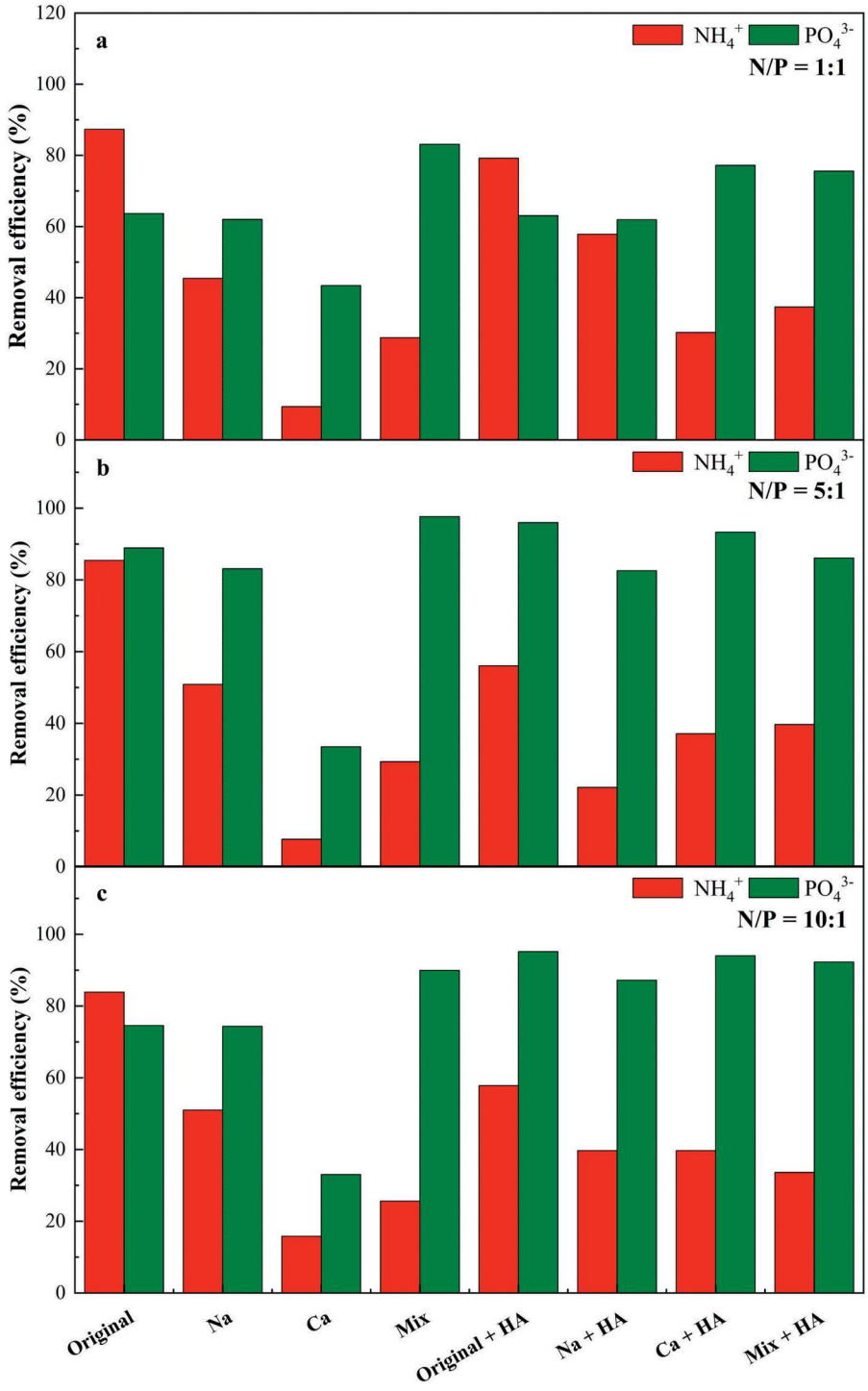

Figure 5. Variation in the removal efficiency of NH_4^+ and PO_4^{3-} after electrolysis at N/P molar ratios of (a) 1:1, (b) 5:1, and (c) 10:1 with 0.7 A, pH 6.0 to 8.0 ± 0.5 of 30 min operational time.

The addition of HA consistently altered struvite crystal morphology and reduced the crystal growth rate [25]. In that case, the induction time of struvite formation in the presence of HA seven times slower than the induction time without HA. Similarly, the growth rate dropped from $(13.8 \pm 0.9) \times 10^{-6}$ to $(7.3 \pm 0.2) \times 10^{-6}$ mol·min^{-1}. This phenomenon explains the complicated interaction between HA and co-cations in the solution. During the primary crystallization phase, HA adsorbed onto the struvite nucleus, inhibiting the development of specific crystal faces. Although crystallization proceeded, the presence of HA on the crystal surface destabilized growth and altered crystal morphology. In the secondary phase, increased aggregation and shear stress further disrupted crystal development, leading to the formation of amorphous, rounded structures. The balance between

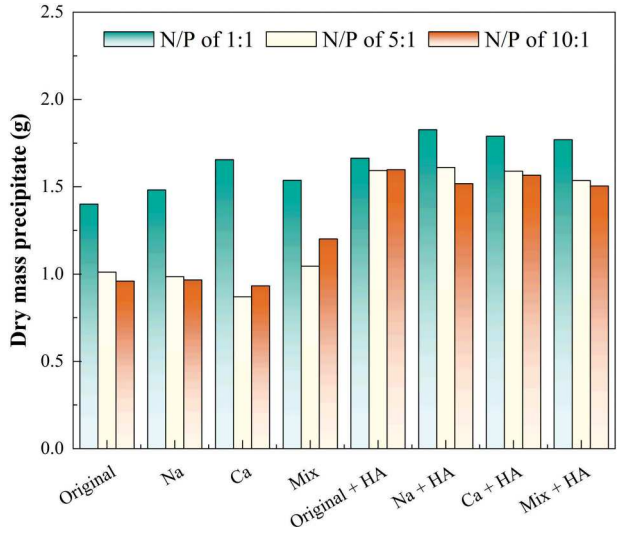

Figure 6. Dry mass of precipitates formed after electrolysis at various N/P molar ratios with and without coexisting ions and HA conditions.

adhesive and drag forces also influenced crystal shape. At such a conditions, stronger adhesive forces produced larger trapezoidal prisms, whereas dominant drag forces yielded smaller crystals [29].

In the Ca^{2+} and Mix variation (both with or without HA), struvite crystals were less distinguishable due to coverage by amorphous phases (Figure 7(c,d)) and (Figure 8(c,d)). Calcium ions competed with Mg^{2+} for PO_4^{3-}, favouring the formation of calcium phosphate phases such as amorphous calcium phosphate (ACP) and hydroxyapatite ($Ca_5(PO_4)_3OH$), rather than struvite [30–32]. High Ca^{2+} concentrations (>100 mg/L) have been reported to reduce struvite crystal size by 40–50% and inhibit nucleation entirely when the Mg:Ca ratio falls below 1:1.4 [33,34]. Under these conditions, any remaining struvite or agglomerates tend to be coated with ACP. Moreover, Ca^{2+} adsorption on struvite surfaces can trigger dissolution–reprecipitation

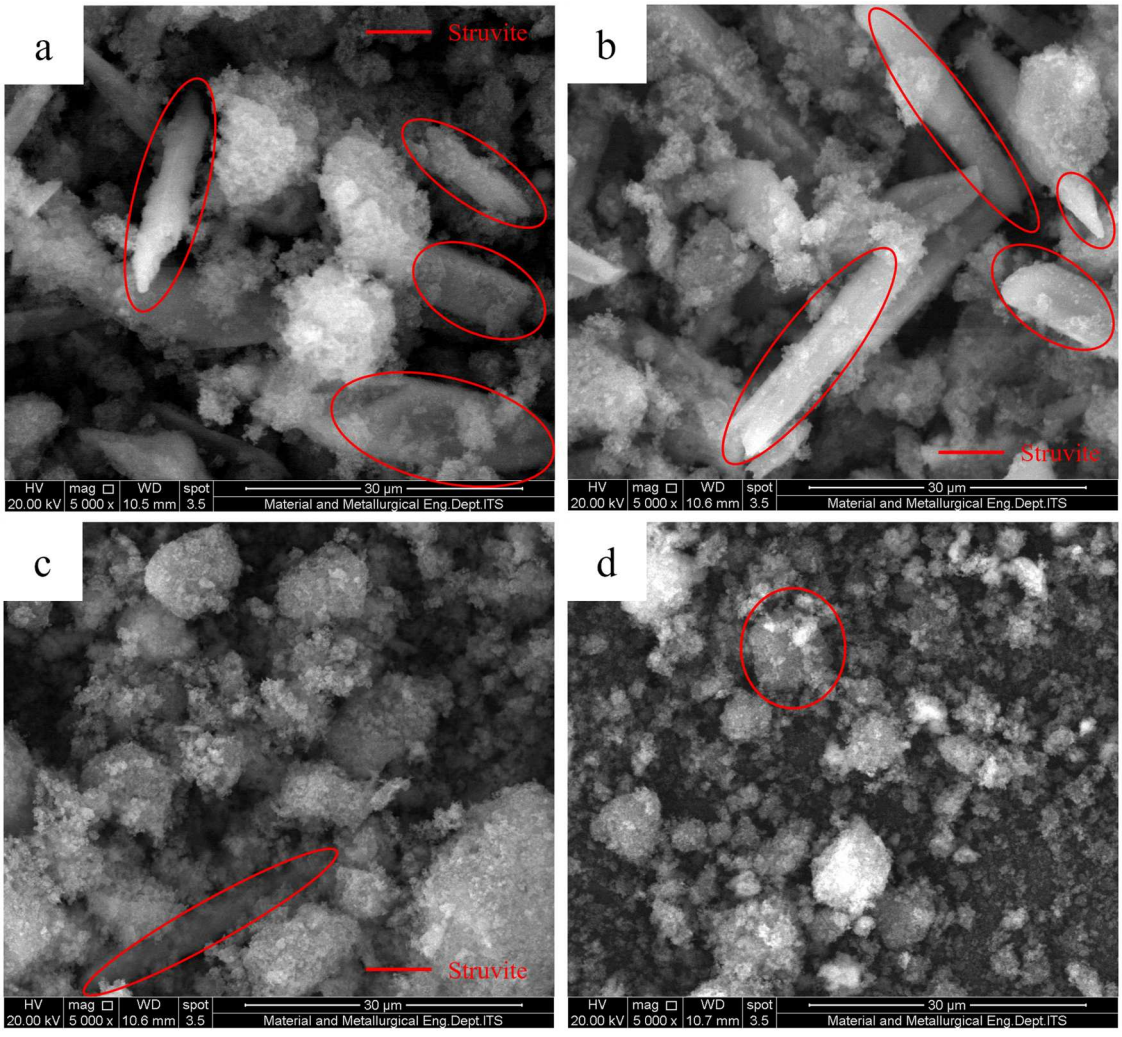

Figure 7. Crystal morphology of precipitate in the variation of (a) Original, (b) Na, (c) Ca, and (d) Mix.

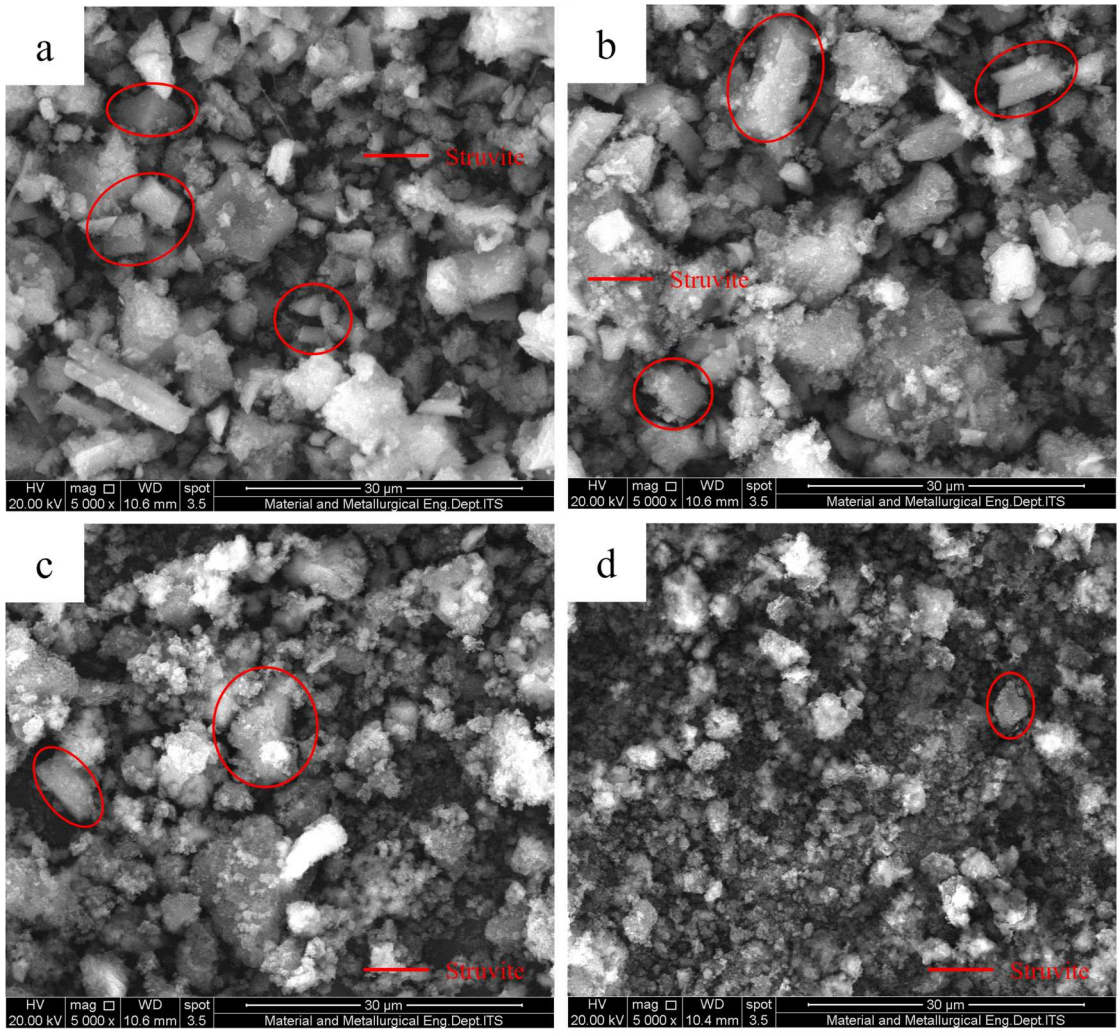

Figure 8. Crystal morphology of precipitate in the variation of (a) Original+HA, (b) Na+HA, (c) Ca+HA, and (d) Mix+HA.

mechanisms, leading to the formation of acidic ACP, which may subsequently transform into monetite ($CaHPO_4$). This transformation depletes available PO_4^{3-} and further suppresses struvite crystallization [34].

This observation indicates that the presence of calcium ions hinders struvite crystallization, potentially by competing with Mg or PO_4^{3-} ions or by promoting the formation of amorphous calcium-phosphate phases. These findings are consistent with those of Le Corre et al. [32], who reported that calcium presence reduces struvite crystal size and favours amorphous precipitation over crystalline forms.

3.3.2. Energy-Dispersive X-ray (EDX) analysis

EDX analysis was performed to assess the elemental composition of the precipitates (**See Figs. S1 and S2 for EDX details)**. In the Original variation and Na^+ addition conditions, the primary elements detected (e.g. O, Mg, P, and K) were consistent with the expected struvite composition (**Figs. S1(a–b)**). Notably, the absence of Na^+ in the Na variation confirmed the effective removal of this competing ion during the MCDI process. In contrast, the Ca and Mix variations exhibited additional elemental signals, including Ca, Al, and Cl, along with the main struvite-forming elements, i.e. O, Mg, P, and K (**Figs. S1(c–d)**). These findings suggest partial interference in the precipitation pathway, possibly leading to the formation of mixed or alternative phases.

The addition of HA further increased this complexity. In the Original + HA and Na + HA variations, minor peaks corresponding to Ca, Al, Na, and Si were detected alongside the primary elements (**Figs. S2(a–b)**). Similarly, the Ca + HA and Mix + HA variations exhibited peaks for Ca, C, Al, Na, and Si (**Figs. S2(c–d)**). The presence of carbon and silicon is attributed to the incorporation of HA and associated organic matter, whereas trace aluminum likely originated from the surface degradation of the magnesium alloy electrode. Overall, the consistent detection of Mg, P, and O across all samples supports the presence of struvite-like compounds. However, the

co-occurrence of additional elements, particularly in HA- and Ca- containing samples, indicates increased compositional complexity and the potential formation of non-struvite phases. Therefore, XRD analysis was conducted to confirm the crystalline identity and purity of the precipitates formed via MCDI-electrolysis process.

3.3.3. Modelling of precipitate formation using Visual MINTEQ 3.1

Visual MINTEQ 3.1 was used to simulate the precipitation equilibria based on elemental composition obtained from EDX analysis. The concentration of NH_4^+ and PO_4^{3-} were determined experimentally, while the concentrations of other elements were estimated from EDX weight percentages and normalized to the dry mass of precipitates. The model generated saturation index (SI) value, where SI > 0 indicates a thermodynamic tendency toward precipitation, and SI < 0 suggested no precipitation occurs [35,36].

The formation of struvite was predicted, as indicated by SI values greater than zero (**See Tables S1-S8 the detail for Visual MINTEQ simulation results**). In both the Original and Na variations, struvite formation was observed alongside the concurrent precipitation of magnesium phosphate **(Table S1 and S2)**. Upon the addition of Ca^{2+} ions, the simulation showed that hydroxyapatite precipitated first, followed by struvite and magnesium phosphate **(Table S3)**. A similar trend was observed for the Mix variation, in which struvite formed only after the initial precipitation of hydroxyapatite **(Table S4)**. These results indicate that the presence of calcium promotes the formation of more diverse and complex mineral phases than the Original variation. This is likely due to the high reactivity of calcium ions, which readily form stable precipitates, thus limiting the availability of magnesium and phosphate ions required for struvite formation. Further complexity was introduced with the addition of HA, which led to the co-precipitation and transformation of other elements such as Al, Si, and C **(Tables S5–S8)**. The presence of HA reduced the purity of struvite by promoting the formation of metal–organic and metal complexes (e.g. with Al), diverting precipitation toward phases like kaolinite or gibbsite instead of struvite. This observation is consistent with findings in swine wastewater, in which HA complexation interfered with the availability of Mg^{2+}/PO_4^{3-} ions, both of which are critical for struvite nucleation [26].

Based on the modelling results, struvite formation was predicted in all variations except the Ca+HA scenario, where hydroxyapatite dominated the precipitation process. This outcome reinforces the idea that the presence of calcium ions hinders struvite formation by altering ion availability and favouring the formation of alternative mineral phases.

3.3.4. X-ray Diffraction (XRD) analysis

XRD analysis was conducted using Match! Software to identify the crystalline phases in the precipitates and assess the struvite purity. Peak intensity was determined using the Rietveld refinement method. The initial candidate phases were selected based on the elemental composition (Mg, N, P, O, H) and the Visual MINTEQ 3.1 simulation results **(See supplementary materials Fig. S3 for XRD pattern variation)**.

In the Original variation, in which no competitor ions or HA were present, the XRD pattern revealed dominant phases such as $Mg_3(PO_4)_2$ (kovdorskite) and other magnesium phosphate rather than pure struvite. These results suggest that these phases crystallized more rapidly than struvite, constituting only 30.7% of the total precipitate. The presence of amorphous-like structures surrounding the struvite crystals (Figure 7(a) and S3(a)), supports this interpretation. In the Na variation (The presence of stand-alone Na^+), XRD analysis revealed a higher struvite proportion – 41.8% of the total precipitate – alongside $Mg_3(PO_4)_2$ and other phases. This 1.5-fold increase in struvite purity compared to the Original variation is not only attributed to the effective removal of Na^+ by MCDI, but also to Na^+ serving as competing ion for NH_4^+ adsorption (Figure 4). As a results, higher concentrations of NH_4^+ and PO_4^{3-} remained in the effluent of MCDI, providing a more favourable ionic composition for struvite precipitation during electrolysis. These findings are consistent with the observed amorphous features in Figure 7(b) and **S3(b)** and further proven that co-ion dynamics and selective adsorption during MCDI can significantly influence downstream crystal purity.

In the Ca variation (the presence of stand-alone Ca^{2+} ion), hydroxyapatite emerged as the dominant phase, while struvite accounted for only 22.4% of the total precipitate. The other detected phases were corundum, diaspores, gibbsite, $Ca_3(PO_4)_2$, and bobierrite. These results correspond with the amorphous structures shown in Figure 7(c). When both sodium and calcium ions were introduced (Mix variation), the XRD pattern revealed hydroxyapatite and kovdorskite as major phases, with struvite comprising only 20.9% of the total precipitate. Additional compounds such as baricite and $Ca_4H(PO_4)_3 \cdot 3H_2O$ were also identified. The amorphous characteristics observed in **Fig. S3(d)** support these findings, confirming the competitive effects predicted by Visual MINTEQ 3.1.

In the Original + HA variation (humic acid present, no competing ions), XRD revealed that kovdorskite and

disodium rhodizonate crystallized preferentially over struvite, which made up just 9.0% of the total precipitate. Other phases included halloysite, kaolinite, diaspore, spinel, magnesium phosphate, quartz, boehmite, gibbsite, and $Al(OH)_3$. These results correspond with the irregular, amorphous morphology surrounding the struvite crystals in **Figs. S3(e)** and 8(a). The reduced struvite purity is attributed to surface interference from HA, which inhibits crystal growth. In the Na + HA variation, magnesium phosphate and sepiolite dominate the XRD pattern, with struvite comprising only 13.9% of the total precipitate. Additional phases included topaz, kaolinite, magnesium hydrogen phosphate, spinel, boehmite, $Al(OH)_3$, gibbsite, Al_2O_3, diaspore, quartz, chrysotile, and halloysite. These findings are consistent with the amorphous regions observed in Figure 8(b) and the reduced struvite purity compared to the Na-only condition (**Fig. S3(f)**), reinforcing the inhibitory role of HA in struvite crystallization.

In the Ca + HA variation, hydroxyapatite remained the dominant phase, while struvite accounted for only 11.6% of the total precipitate. Additional phases included newberyite, kaolinite, gibbsite, Al_2O_3, boehmite, $Ca(HPO_4)$, halloysite, diaspore, topaz, cristobalite, sepiolite, $Al(OH)_3$, and quartz. These findings align with the amorphous structures shown in Figure 8(c) and demonstrate further suppression in struvite purity compared with the original+HA and Na+HA variations (Fig. S3(g)). In the most complex scenario, the Mix+HA variation (sodium, calcium, and humic acid all present), XRD analysis identified sepiolite, kaolinite, $Ca_3(PO_4)_2$, boehmite, hydroxyapatite, spinel, halloysite, $Al(OH)_3$, gibbsite, and $Ca(HPO_4)\cdot 2H_2O$ as the dominant phases. Struvite constituted only 1.0% of the total precipitate. Minor phases such as diaspore, chrysotile, and newberyite, were also detected. These findings explain the highly amorphous appearance seen in Figure 8(d) and indicate severely inhibited struvite formation due to the reduced quality of the MCDI effluent used during electrolysis (Fig. S3(h)).

3.4. Struvite production and purity assessment

Struvite purity was assessed via 2 different methods, namely stoichiometric calculations and XRD analysis. The stoichiometric approach assumed complete conversion of Mg^{2+}, NH_4^+, and PO_4^{3-} into struvite in a 1:1:1 molar ratio (Equation (7)), whereas the XRD method, supported by EDX data, quantified only the crystalline phases present in the recovered solids. In this study, XRD-based values were prioritized as they more accurately represent the actual crystalline struvite content. As discussed previously, the addition of HA reduced struvite purity, likely due to its adsorption onto crystal surfaces, which interfered with crystal growth.

In the stoichiometric calculations approach, the limiting reagent was identified either NH_4^+ or PO_4^{3-} depending on concentration. The theoretical struvite yield was calculated based on its molar amount. The amount of generated Mg^{2+} during electrolysis was estimated using Faraday's law (Equation (8)) [16], while NH_4^+ and PO_4^{3-} concentrations were determined from the difference between the initial and final concentration after the combined MCDI–electrolysis process.

$$Mg^{2+} + NH_4^+ + PO_4^{3-} + 6H_2O \rightarrow MgNH_4PO_4 \cdot 6H_2O \quad (7)$$

$$m_{Mg} = \frac{M_{Mg} \times I \times t}{z \times F} \quad (8)$$

where m_{Mg} is the theoretical magnesium release (g), A is the atomic weight of magnesium (24.3 $g\cdot mol^{-1}$), I is electric current (A), t is the time elapsed (s), z is magnesium valence (2), and F is the Faraday constant (96,485 $C\cdot mol^{-1}$).

Based on Equation (8), 0.158 g (6.53 mmol) of Mg^{2+} was released during the 30 min process. The molar quantity was then multiplied by molar mass of struvite (245.4 $mg\cdot mol^{-1}$). Theoritical struvite yield was then calculated and divided by the actual recovered mass to estimate struvite purity based on stoichiometry calculation (Figure 9).

Stoichiometric calculations revealed that HA consistently reduced struvite purity across all experimental conditions. The Original variation achieved the highest purity at around 1.4 g (nearly 100%), which lacked competing ions and HA. In contrast, stand-alone HA (Original + HA) decreased purity to 89.55% (1.4895 g), indicating an inhibitory effect of HA on crystal formation. Among the variations containing competing ions, Na and Na + HA cases showed relatively high purities, accounting for 84.61% (1.254 g) and 77.91% (1.423 g), respectively. These results suggest that Na^+ improves struvite formation.

XRD analysis further corroborated these findings. Under the Original condition, the struvite accounted for 30.97% of the crystalline product, increasing to 41.80% with Na^+ addition. In contrast, Ca^{2+} significantly reduced struvite purity for approximately 22.40% and 20.90% for the mixed Na^+ and Ca^{2+} conditions. HA further suppressed struvite crystallization in all scenarios. Regardless of the ideal conditions (Original and Original + HA), the Na variation yielded the highest crystalline struvite content for approximately 41.80% (0.6195 g). These results indicate that while Na^+ may enhance

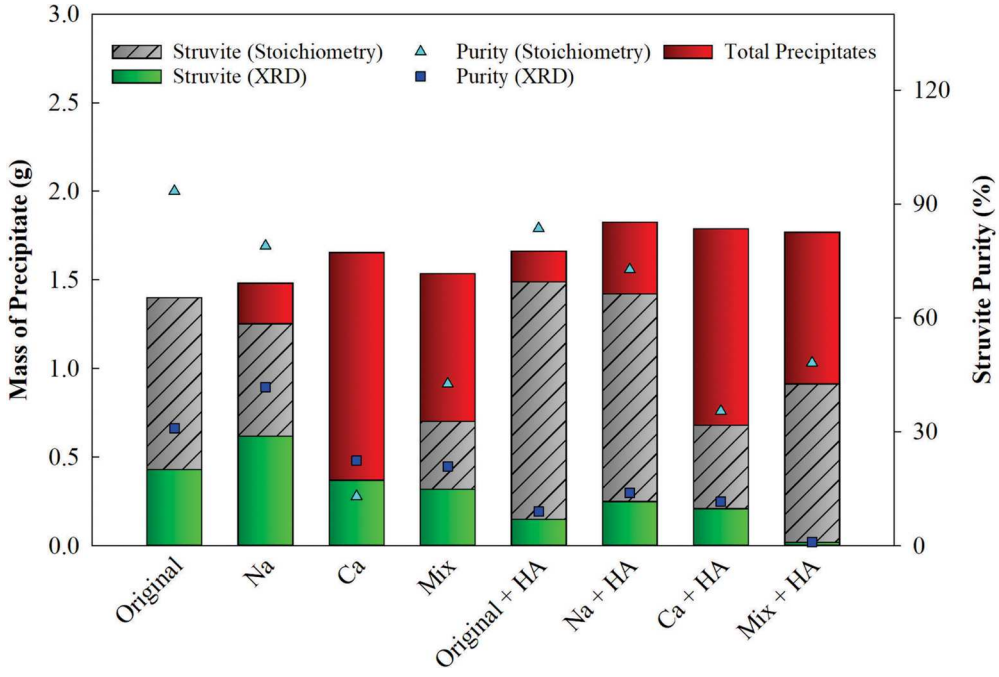

Figure 9. Generated precipitate after MCDI-electrolysis process and purity of struvite based on theoretical calculations via stoichiometry and actual value from XRD survey results.

struvite purity, Ca^{2+} and HA strongly inhibit the formation of struvites with high purity.

3.5. Energy consumption

The energy consumption of the combined MCDI and electrolysis process for struvite formation was evaluated to assess overall energy efficiency at **Fig. S4 (See supplementary materials for the detail of energy consumption variation across all processes)**. The MCDI process exhibited relatively low energy consumption, ranging from 0.06 to 0.22 Wh across all N/P molar ratios. At these moments, the presence of coexisting ions and HA in the solution led to a moderate increase in energy consumption **(Fig. S4(a))**. In contrast, the 30-min electrolysis process required significantly more energy, ranging from 6.87 to 19.61 Wh, depending on the N/P molar ratio **(Fig. S4(b))**. Despite this, the total energy consumption per gram of precipitate remained relatively low, particularly at an N/P molar ratio of 1:1, with values between 4.32 and 5.51 $Wh{\cdot}g^{-1}$ of precipitate. However, increasing the N/P molar ratio to 1:5 and 10:1 resulted in higher total energy consumption, reaching up to approximately 15.88 $Wh{\cdot}g^{-1}$ of precipitate **(Fig. S4(c))**. The highest energy consumption was recorded at an N/P ratio of 10:1 in the absence of coexisting ions and HA as high as 15.88 $Wh{\cdot}g^{-1}$.

A previous study has demonstrated a substantially higher energy requirement of 146.96 $Wh{\cdot}g^{-1}$ for a similar process using simulated wastewater [14]. The use of energy consumption can be more efficiently managed by maintaining a low applied current, as shown by a previous study that applying low current at 10 mA during the treatment, can achieve low-energy consumption as low as 1.64 $Wh{\cdot}g^{-1}$ by an electrolysis process to treat 200 mL of simulated wastewater [37]. These comparisons indicated that the combined process investigated in the present study considerably improved struvite formation. Although traditional chemical precipitation processes consume less energy, their reliance on chemical inputs and the production of secondary waste streams can undermine economic viability. The study suggests that combining MCDI and electrolysis provides a practical and energy-efficient approach for nutrient recovery and struvite precipitation, especially when stoichiometric conditions are optimized.

3.6. Limitations and practical implications for application in real wastewater

Although this study demonstrates the potential of MCDI-electrolysis integration for struvite recovery, several limitations should be noted. Synthetic wastewater was used to create controlled conditions, which simplifies the ionic composition and complexity of organic matter compared to real wastewater. In practice, municipal and industrial wastewaters contain a broader range of ions (e.g. bicarbonate, sulfate, potassium) and diverse organic substances that may interfere with ion

transport, precipitation kinetics, and crystal purity. This study proves that co-existing ions (i.e. Ca^{2+} and HA) can significantly alter struvite morphology and reduce purity. Additionally, scale-up challenges such as electrode degradation, and membrane fouling must be addressed. Electrode lifetime may be reduced under continuous operation, while system fouling can impair performance. To improve process applicability, future research should focus on pilot-scale testing using actual wastewater, evaluating long-term stability, regeneration protocols, and economic feasibility. Strategies such as selective ion removal, Mg supplementation, struvite morphology identification (size ranges measurement), pH control, and predictive modelling, which use of mathematical, statistical, or computational techniques to forecast or simulate outcomes based on input variables, may enhance struvite selectivity and yield in complex matrices.

Despite these challenges, the integrated MCDI-electrolysis system offers significant benefits for energy-efficient nutrient recovery such as struvite as a valuable slow-release fertilizer. This modular combined system allows easy integration into existing infrastructure, improving effluent quality to meet stringent discharge standards.

4. Conclusion

This study has demonstrated that integrating MCDI with Mg-based electrolysis significantly enhances struvite formation for nutrient recovery from wastewater. The combined process using an AZ31B Mg alloy sacrificial anode achieved NH_4^+ and PO_4^{3-} removal efficiencies up to 4 to 5 times greater than MCDI alone, primarily due to controlled struvite precipitation. However, the presence of competing ions particularly Ca^{2+} and organic substances such as HA negatively influenced ion electrosorption and crystal purity by introducing fouling, surface blockage, and ion competition. The N/P molar ratio was a key determinant in optimizing struvite yield and purity with the highest crystalline struvite content (41.80% or 0.62 g) observed under stand-alone Na^+ variation. The integrated system also exhibited favourable energy performance with an energy consumption as low as 4.32 $Wh{\cdot}g^{-1}$ under stoichiometric balance. Beyond lab-scale outcomes, this study holds strong potential for scalable implementation in real-world treatment applications, enabling on-site nutrient recovery and reducing reliance on conventional fertilizers. Its compatibility with existing infrastructure, alignment with circular economy principles. Despite promising results under synthetic conditions, real wastewater presents additional complexity due to variable ionic composition and operational challenges such as electrode degradation, membrane fouling, and system instability. Future work should focus on pilot-scale validation with actual wastewater streams, along with strategies for system optimization, including selective ion removal, pH control, and predictive modelling to support scalable and energy-efficient nutrient recovery in full-scale wastewater treatment applications.

CRediT authorship contribution

Aditya Kurnia Aji Pangestu: Writing – original draft, Investigation, Formal analysis, Visualization. Arseto Yekti Bagastyo: Resources, Conceptualization, Project administration, Writing – review & editing, Supervision, Funding acquisition. Ervin Nurhayati: Resources, Data curation, Methodology, Writing – review & editing, Supervision. Jr-Lin Lin: Resources, Conceptualization, Supervision, Methodology. Fahrudin Sidik: Writing – review & editing, Supervision, Methodology, Data curation.

Disclosure statement

No potential conflict of interest was reported by the author(s).

Funding

The authors would like to acknowledge the Ministry of Education, Culture, Research, and Technology of the Republic of Indonesia for the financial support (038/E5/PG.02.00.PL/2024 and 1740/PKS/ITS/2024) under the Fundamental Research Scheme.

Data availability statement

Data sharing is not applicable to this article.

ORCID

Arseto Yekti Bagastyo http://orcid.org/0000-0001-8850-9255
Ervin Nurhayati http://orcid.org/0000-0001-8812-2034
Fahrudin Sidik http://orcid.org/0000-0002-5747-1546

References

[1] Ye Y, Ngo HH, Guo W, et al. A critical review on ammonium recovery from wastewater for sustainable wastewater management. Bioresour Technol. 2018;268(June):749–758. doi:10.1016/j.biortech.2018.07.111

[2] Zhou Y, Wang J. Detection and removal technologies for ammonium and antibiotics in agricultural wastewater: recent advances and prospective. Chemosphere. 2023;334(May):139027.

[3] Zhang G, Li W, Wang S, et al. Evaluation of various carbon sources on ammonium assimilation and denitrifying phosphorus removal in a modified anaerobic-anoxic-oxic process from low-strength wastewater. Sci Total Environ. 2024;926(September 2023):171890.
[4] Fizir M, Touil S, Richa A, et al. Kaolin-iron cross-linked alginate beads for efficient phosphate removal from water: An initiation towards sustainable treatment of domestic and hydroponic wastewaters. Appl Clay Sci. 2024;256 (May):107430.
[5] Xiao Q, Ma J, Xu L, et al. Membrane capacitive deionization (MCDI) for selective ion separation and recovery: fundamentals, challenges, and opportunities. J Memb Sci. 2024;699(December 2023):122650.
[6] Biesheuvel PM, van der Wal A. Membrane capacitive deionization. J Memb Sci. 2010;346(2):256–262. doi:10.1016/j.memsci.2009.09.043
[7] Wimalasiri Y, Mossad M, Zou L. Thermodynamics and kinetics of adsorption of ammonium ions by graphene laminate electrodes in capacitive deionization. Desalination. 2015;357:178–188. doi:10.1016/j.desal.2014.11.015
[8] Sakar H, Celik I, Balcik-Canbolat C, et al. Ammonium removal and recovery from real digestate wastewater by a modified operational method of membrane capacitive deionization unit. J Clean Prod. 2019;215:1415–1423. doi:10.1016/j.jclepro.2019.01.165
[9] Jiang J, Dorji P, Badeti U, et al. Potential nutrient recovery from source-separated urine through hybrid membrane bioreactor and membrane capacitive deionisation. Desalination. 2023;566(August):116924.
[10] Talboys PJ, Heppell J, Roose T, et al. Struvite: a slow-release fertiliser for sustainable phosphorus management? Plant Soil. 2016;401(1–2):109–123. doi:10.1007/s11104-015-2747-3
[11] Valle SF, Giroto AS, Dombinov V, et al. Struvite-based composites for slow-release fertilization: a case study in sand. Sci Rep. 2022;12(1):1–14. doi:10.1038/s41598-021-99269-x
[12] Min KJ, Kim D, Lee J, et al. Characteristics of vegetable crop cultivation and nutrient releasing with struvite as a slow-release fertilizer. Environ Sci Pollut Res. 2019;26(33):34332–34344. doi:10.1007/s11356-019-05522-2
[13] González C, Fernández B, Molina F, et al. The determination of fertiliser quality of the formed struvite from a WWTP. Water Sci Technol. 2021;83(12):3041–3053. doi:10.2166/wst.2021.162
[14] Wang L, Gu K, Zhang Y, et al. Enhanced struvite generation and separation by magnesium anode electrolysis coupled with cathode electrodeposition. Sci Total Environ. 2022;804:150101.
[15] Siciliano A, Limonti C, Curcio GM, et al. Advances in struvite precipitation technologies for nutrients removal and recovery from aqueous waste and wastewater. Sustain. 2020;12(18):7538.
[16] Bagastyo AY, Anggrainy AD, Khoiruddin K, et al. Electrochemically-driven struvite recovery: prospect and challenges for the application of magnesium sacrificial anode. Sep Purif Technol. 2022;288(November 2021):120653.
[17] Luo W, Fang Y, Song L, et al. Production of struvite by magnesium constant voltage electrolytic crystallisation from anaerobically digested chicken manure slurry. Environ Res. 2022;21:113991, 1–10. doi:10.1069/j.envres.2022.113991.
[18] Qu Y, Campbell PG, Gu L, et al. Energy consumption analysis of constant voltage and constant current operations in capacitive deionization. Desalination. 2016;400:18–24. doi:10.1016/j.desal.2016.09.014
[19] Hou CH, Taboada-Serrano P, Yiacoumi S, et al. Electrosorption selectivity of ions from mixtures of electrolytes inside nanopores. J Chem Phys. 2008;129:224703.
[20] Chen Z, Zhang H, Wu C, et al. A study of electrosorption selectivity of anions by activated carbon electrodes in capacitive deionization. Desalination. 2015;369:46–50. doi:10.1016/j.desal.2015.04.022
[21] Wang Q, Fang K, He C, et al. Ammonia removal from municipal wastewater via membrane capacitive deionization (MCDI) in pilot-scale. Sep Purif Technol. 2022;286(December 2021):120469.
[22] Chen L, Wang C, Liu S, et al. Investigation of the long-term desalination performance of membrane capacitive deionization at the presence of organic foulants. Chemosphere. 2018;193:989–997. doi:10.1016/j.chemosphere.2017.11.130
[23] Jing J, Zhang S, Yuan L, et al. Combining humic acid with phosphate fertilizer affects humic acid structure and its stimulating efficacy on the growth and nutrient uptake of maize seedlings. Sci Rep. 2020;10(1):1–10. doi:10.1038/s41598-019-56847-4
[24] Warmadewanthi RA, Ikhlas N, et al. The effect of mixing rate on struvite recovery from the fertilizer industry. IOP Conf Ser Earth Environ Sci. 2020;506(1):012013. doi:10.1088/1755-1315/506/1/012013
[25] Wei L, Hong T, Cui K, et al. Probing the effect of humic acid on the nucleation and growth kinetics of struvite by constant composition technique. Chem Eng J. 2019;378(June):122130.
[26] Chen RF, Liu T, Rong HW, et al. Effect of organic substances on nutrients recovery by struvite electrochemical precipitation from synthetic anaerobically treated swine wastewater. Membranes (Basel). 2021;11(8):594.
[27] Zhang Q, Zhao S, Ye X, et al. Effects of organic substances on struvite crystallization and recovery. Desalin Water Treat. 2016;57(23):10924–10933. doi:10.1080/19443994.2015.1040850.
[28] Zhou Z, Hu D, Ren W, et al. Chemosphere effect of humic substances on phosphorus removal by struvite precipitation. Chemosphere. 2015;141:94–99.
[29] Pavez-jara J, Iswarani WP, Lier JV, et al. Role of the composition of humic substances formed during thermal hydrolysis process on struvite precipitation in reject water from anaerobic digestion. J Water Process Eng. 2024;59(January):104932.
[30] Hutnik N, Piotrowski K, Wierzbowska B, et al. Continuous reaction crystallization of struvite from phosphate (V) solutions containing calcium ions. Cryst Res Technol. 2011;449:443–449.
[31] Enyemadze I. Review paper phosphorus recovery by struvite precipitation: a review of the impact of calcium on struvite quality. J Water, Sanitation Hyg Dev. 2021;11(5):30–37.

[32] Le Corre KS, Valsami-Jones E, Hobbs P, et al. Impact of calcium on struvite crystal size, shape and purity. J Cryst Growth. 2005;283(3–4):514–522. doi:10.1016/j.jcrysgro.2005.06.012

[33] Hutnik N, Stanclik A, Piotrowski K, et al. Size-dependent growth kinetics of struvite crystals in wastewater with calcium ions. Open Chemistry. 2020;18(1):196–206.

[34] Qin L, Putnis CV, Wang L. Facet-Specific dissolution – Precipitation at struvite – Water interfaces. Cryst Growth Des. 2021;21(7):4111–4120.

[35] Hug A, Udert KM. Struvite precipitation from urine with electrochemical magnesium dosage. Water Res. 2013;47(1):289–299. doi:10.1016/j.watres.2012.09.036

[36] Li B, Boiarkina I, Yu W, et al. Phosphorous recovery through struvite crystallization: challenges for future design. Sci Total Environ. 2019;648:1244–1256. doi:10.1016/j.scitotenv.2018.07.166

[37] Natsi PD, Koutsoukos PG. Electrochemical recovery of N and P from municipal wastewater. Crystals. 2024;14(8):675. doi:10.3390/cryst14080675